Part I

Polarimetry

Oh all of the questions
All of the stars in the sky
Oh never the answers
Always the wondering why

"I Would I Were" by James Keelaghan

Chapter 2

Observing Particulars

2.1 Telescopes and Receivers

2.1.1 Green Bank 140′

The 800-MHz and 575-MHz polarimetric data presented in this thesis were all obtained at the NRAO 140′ (43m) telescope at Green Bank, WV. This telescope has an equatorial mount, which means the orientation of the feed remains fixed with respect to the source. The feed must be rotated manually in order to deal with polarization calibration issues (cf. section 2.5.2).

The 300-1000 MHz and 1000-1450 MHz prime focus receivers were used for these observations. At 800 and 1400 MHz dual orthogonal linear polarizations were received, amplified, and passed through a quadrature hybrid device for conversion to left and right hand circular polarizations. Independent linearly-polarized diode noise sources were injected prior to the first stage of amplification for secondary calibration purposes. At 575 MHz the hybrid is immediately after the feed, and the independent noise sources are therefore circularly polarized. A correlated noise source was injected prior to the hybrid for these observations. The radio frequency (RF) signals centered at 800 MHz were mixed with a local oscillator (LO) to an intermediate frequency (IF) of 250 MHz, and passed through 80-MHz bandpass filters. The GBPP (cf. section 2.2.1) requires an IF near 400 MHz. The signals were therefore converted to an IF of 420 MHz by mixing with another LO, and passed through another 80-MHz bandpass filter centered at 400 MHz. Our 28-MHz observing band was centered at 400 MHz, corresponding to an RF of 820 MHz. The 575-MHz RF signals were mixed with an LO to an IF of 250 MHz, passed through 80-MHz bandpass filters, converted to an IF of 400 MHz with another LO, and and passed through another set of 80-MHz bandpass filters. Our 28-MHz observing band was centered at a sky radio frequency of 575-MHz.

Typical system temperatures for the 575, 800, and 1400-MHz observations are

60-70K, 40-60K and 20-25K respectively, with antenna gains of 0.25-0.3 K Jy^{-1}.

2.1.2 Green Bank 85-3

The Green Bank 85-3 was one element of an interferometer consisting of three 25-m telescopes. This telescope is now used as a pulsar monitoring telescope, and was used to obtain polarization data for the Crab pulsar. Two linearly polarized 610-MHz signals are mixed to an IF of 400 MHz, and passed to the GBPP.

2.1.3 Effelsberg 100m

The 100-m telescope at Effelsberg, Germany was used for the 1400 MHz observations presented here. The alt-azimuth mount of this telescope results in an automatic rotation of the feed relative to the sky. This *parallactic angle* must be included in the processing of any observations. The 1.41-GHz HEMT receiver located at the prime focus is tunable between 1.3 and 1.7 GHz. The antenna gain at these frequencies is 1.5 K Jy^{-1}, independent of elevation. Dual orthogonal linear polarizations are received, amplified, and passed through a quadrature hybrid device for conversion to left and right hand circular polarizations, following the NRAO design. A single linearly polarized noise source is injected prior to the hybrid for calibration purposes. These incoming radio frequency signals were passed through bandpass filters centered at 1415 MHz which have a 130-MHz bandwidth. The 1410-MHz signals were mixed to an IF of 150 MHz. This IF was passed to the EBPP, which immediately mixed the signals with another LO to an IF of 440 MHz. Our observing bandwidth (28 MHz) was centered at 1410 MHz. The system temperature was 35-50K for these observations.

2.2 Berkeley Pulsar Processors

The effects of interstellar dispersion discussed in section 1.8.1 are most troublesome for short period objects, where the dispersion across even a relatively narrow band can be a significant fraction of a pulse period. Traditionally, the incoming signal has been divided up into many separate narrow frequency channels, within which the dispersion smearing is no larger than the desired temporal resolution. The signal in each channel is later delayed by the expected dispersion delay prior to averaging over the channels. For high resolution profiles at short periods, the channels must become very narrow, limiting the total bandwidth which may be used. An alternative approach has been to record fast-sampled raw voltage data. The effects of interstellar dispersion amount to a frequency-dependent phase rotation of the complex voltages. This complex multiplication in the frequency domain, or convolution in the time domain, may be removed in software prior to detection (Hankins 1971, Hankins & Rickett 1975). This coherent dedispersion technique results in high time resolution, but requires significant computer resources. The Berkeley Pulsar Processors were developed to perform the deconvolution in real-time, to simplify later processing.

2.2.1 GBPP

The Green Bank-Berkeley Pulsar Processor (GBPP) was originally called the Coherent Dispersion Removal Processor, or CDRP. The CDRP was designed for sensitive high resolution timing and polarimetry observations of short period, highly dispersed pulsars. The effects of interstellar dispersion are removed via complex convolution in the time domain. The GBPP currently consists of 32 frequency channels for each polarization. It can remove up to 1024 time samples of dispersion per channel for channel bandwidths up to 1 MHz. The channel widths can be set in steps of 1.414, and full Stokes parameters can be analyzed for channel bandwidths up to 0.875 MHz. Other observing modes allow channel bandwidths up to 4 MHz for intensity observations. The minimum time resolution in the pulse profile for polarization observations is one of (a) period/2048; (b) inverse of the channel bandwidth, whichever is largest.

The CDRP was designed and constructed by the Berkeley Pulsar Group, starting with support from the NSF Science & Technology Center for Particle Astrophysics. In 1994 a half system (16 channel) CDRP-0 was brought to Green Bank. This system was used for some initial polarization observations. In 1995 a full system CDRP-2 was brought to Green Bank. In 1996 the designed CDRP-2 system was completed with the addition of an agile analog stage of electronics. CDRP-2 normally resides at the 85′ telescope, and was used for the small amount of polarimetric data taken with

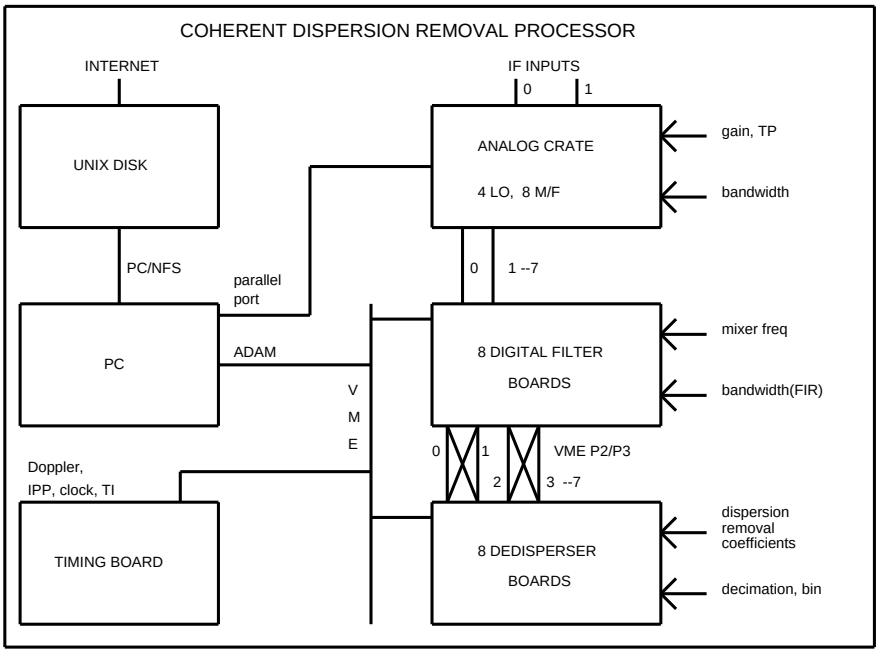

Fig. 2.1.— A block diagram of the Berkeley Pulsar Processor. This coherent dispersion removal processor has an analog crate and 8 digital filter boards to channelize the data, which is dedispersed, detected, and averaged by the dedisperser boards. The timing board synchronizes the system, which is controlled by a PC.

this telescope. CDRP-2 was renamed GBPP to provide uniformity amongst other processors completed or under construction. This processor was used for all of the 575-MHz observations and the majority of the 800-MHz observations. Up to 28 MHz of bandwidth could be used for the polarization observations.

The GBPP consists of Analog and Digital Crates for channelization, dispersion removal, detection and signal averaging. A schematic diagram showing the major components of the GBPP is shown in Figure 2.1. The analog crate divides the incoming signal for each polarization into 4 bands, mixing each to baseband. The Digital Filter Boards (DFBs) divide each of these bands into 8 individual channels, resulting in 32 channels per polarization. Four channels of each polarization (from two DFBs) are passed to a single Dedisperser Board (DB) for processing. On each DB, a VLSI device developed by Amar Kapadia *et al.* (1993) performs a 1024-point complex deconvolution of the dispersion effects of the interstellar plasma. This is followed by detection of the signal (and cross-detection to generate the Stokes parameters), and averaging synchronously with the pulse period. The Timing Board controls the DFBs

and DBs, tracks the apparent pulsar period, and communicates with the PC which controls the system. The A/D (analog to digital) portion of the system has 4-bit output, while the DFB output is 2-bit. This results in a non-linear power correction which must be applied to the data during processing. A partial technical description of the GBPP, focussing on the DFB, may be found in Backer *et al.* (1997).

2.2.2 EBPP

The Effelsberg-Berkeley Pulsar Processor (EBPP) is a clone of the GBPP, and was used for the 1400-MHz observations. The first half of the system (16 channels) was installed at the Effelsberg 100m telescope in 1996 October (denoted EBPP-a in table 2.1), and a limited amount of polarimetry data was obtained at that time. The system was completed before the remainder of the observations in Spring 1997.

2.3 Observing information

Polarimetry observations were obtained at several epochs. The 575-MHz data were all obtained at Green Bank in 1997 July, in a run dedicated to polarization. The 800-MHz data were obtained in 1995 January/February, 1997 February, April, and July. Most of these data were obtained during standard pulsar timing runs (see Foster & Backer 1990 for a description of the Pulsar Timing Array program) which use the Spectral Processor; therefore a limited amount of calibration was possible for these data. Due to concerns about instrumental effects introduced by the hybrid, the hybrid was removed from the system for the 1995 data, resulting in dual linear polarizations. The 1400-MHz data were obtained at Effelsberg in 1996 October, 1997 March/April.In addition, we present polarimetry of the Crab pulsar at 610 MHz, taken at the 85-3 telescope in Green Bank, WV.

The dates of observation are displayed for each pulsar in table 2.1, along with the radio frequency in MHz, channel bandwidth in MHz, number of channels available, the polarization system used, and the processor which obtained the data. In all cases, the raw data consists of scans with 16 or 32 frequency channels, up to 2048 time bins, and 4 polarizations, each having an integration time of 2 to 15 minutes (usually near 5 minutes). The data were inspected for interference, and problem scans and channels were removed from further consideration.

In order to produce a polarization profile for a given pulsar at a given frequency, gain calibration (cf. section 2.4) must be applied, the instrumental polarization effects of the telescope must be removed (cf. section 2.5), any polarization position angle offsets between different sets of data must be removed, and the scans must be temporally aligned (cf. section 2.6).

Summary of Observations

Source	Dates	Freq MHz	CBW MHz	Chans	Poln Sys	Observing System
B0531+21	1996 11/13-4,27,30, 12/2	610	0.5	32	lin	GBPP
J0613-0200	1997 7/28-9	575	0.70	32	circ	GBPP
J0613-0200	1995 1/30-1, 2/06-7	800	0.70	16	lin	CDRP-0
J0613-0200	1997 2/10-1, 4/26,28-9, 7/31-8/01	820	0.875	32	circ	GBPP
J0613-0200	1997 4/09	1410	0.875	32	circ	EBPP
J0751+1807	1997 3/19	1410	0.875	32	circ	EBPP
J1012+5307	1997 7/25-9	575	0.875	32	circ	GBPP
J1012+5307	1997 2/10-2, 4/26-9, 7/31-8/01	820	0.875	32	circ	GBPP
J1012+5307	1996 10/15	1410	0.7	16	circ	EBPP-a
J1012+5307	1997 3/19	1410	0.875	32	circ	EBPP
J1012+5307	1997 4/09	1410	0.875	32	circ	EBPP
J1022+1001	1997 7/25-8	575	0.875	32	circ	GBPP
J1022+1001	1997 2/12, 4/27-30, 7/31	820	0.875	32	circ	GBPP
J1022+1001	1996 10/05	1410	0.7	12	circ	EBPP-a
J1022+1001	1997 3/19, 4/09	1410	0.875	32	circ	EBPP
J1518+4904	1997 3/19	1410	0.875	32	circ	EBPP
B1620-26	1997 7/26-30	575	0.50	32	circ	GBPP
B1620-26	1997 2/10-2, 4/26-30, 7/30-8/01	820	0.875	32	circ	GBPP
B1620-26	1995 1/31, 2/06	800	0.70	16	lin	CDRP-0
B1620-26	1995 2/05	800	0.70	16	circ	CDRP-0
B1620-26	1997 3/20,24,4/10	1410	0.875	32	circ	EBPP
J1640+2224	1997 3/24, 4/10	1410	0.875	32	circ	EBPP
J1643-1224	1997 3/20, 4/10	1410	0.875	32	circ	EBPP
J1713+0747	1997 7/25-30	575	0.875	32	circ	GBPP
J1713+0747	1997 2/10-2, 4/26-30, 7/30-1	820	0.875	32	circ	GBPP
J1713+0747	1995 1/30-1, 2/05-7	800	0.70	16	lin	CDRP-0
J1713+0747	1995 2/05	800	0.70	16	circ	CDRP-0
J1713+0747	1997 3/19-20, 4/09	1410	0.875	32	circ	EBPP
J1730-2304	1997 7/29-30	575	0.875	32	circ	GBPP
J1730-2304	1997 2/10-1, 4/26-7, 7/31-8/01	820	0.875	32	circ	GBPP
J1730-2304	1997 4/10	1410	0.875	32	circ	EBPP
B1821-24	1997 7/25-30	575	0.35	32	circ	GBPP
B1821-24	1997 2/10-1, 4/26-30, 7/31-8/01	820	0.70	32	circ	GBPP
B1821-24	1997 3/20,24, 4/10	1410	0.875	32	circ	EBPP
B1937+21	1997 7/24-30	575	0.50	32	circ	GBPP
B1937+21	1997 2/10-1, 4/26-9, 7/31-8/01	820	0.875	32	circ	GBPP
B1937+21	1995 1/31	800	0.70	16	lin	CDRP-0
B1937+21	1995 2/05-7	800	0.70	16	lin	CDRP-0
B1937+21	1997 3/19-20,24, 4/10	1410	0.875	32	circ	EBPP
J2145-0750	1997 7/25-30	575	0.875	32	circ	GBPP
J2145-0750	1997 2/10-1, 4/26-9, 7/31-8/01	820	0.875	32	circ	GBPP
J2145-0750	1995 1/29-31, 2/05-6	800	0.70	16	lin	CDRP-0
J2145-0750	1995 2/04	800	0.70	16	circ	CDRP-0
J2145-0750	1997 4/10	1410	0.875	32	circ	EBPP

Table 2.1: **Observing Information for Millisecond Pulsars.** For each pulsar, the observing dates, radio frequency in MHz, the channel bandwidth in MHz of the BPP, and the number of channels are listed in columns 2-4. Columns 5 and 6 indicate whether the data were taken in the linear or circular polarization basis, and the observing system which recorded the data.

2.4 Gain Calibration

The data obtained using two orthogonal polarizations A and B must be converted from raw data counts to flux units for each polarization. Observations of a calibrated pulsed noise source allow the determination of the number of counts per CAL deflection. Pulsed noise observations both on and off an unpolarized standard source of known flux F then allow determination of the flux per CAL deflection, and therefore per count. This gain factor g_i is determined for each polarization i in Jy/c, and may then be applied to the data.

If the noise source has a known temperature T_{CAL_i} in polarization i, then we can determine the *system temperature* T_{SYS_i}, the antenna temperature T_{ANT_i}, and the *antenna gain* G_i in K/Jy for the observations. The Kelvins per count for polarization i, $(K/c)_i$, is determined by

$$(K/c)_i = \frac{T_{CAL_i}}{(counts(CAL_{ON}) - counts(CAL_{OFF}))_i}, \tag{2.1}$$

and the system temperature is given by

$$T_{SYS_i} = (K/c)_i \cdot counts(CAL_{OFF_i}). \tag{2.2}$$

Observations of the system temperatures both ON and OFF an unpolarized standard source of known flux F gives the antenna temperature

$$\begin{aligned} T_{ANT_i} &= T_{SYS_i}(ON) - T_{SYS_i}(OFF) \\ &= (K/c)_i \cdot (counts(ON) - counts(OFF))_i, \end{aligned} \tag{2.3}$$

and the gain G_i of the telescope in Kelvins per Jansky:

$$G_i = \frac{T_{ANT_i}}{F}. \tag{2.4}$$

The overall gain factor g_i in Jy/c,

$$g_i = (K/c)_i / G_i \tag{2.5}$$

may then be applied to each polarization i of the data. The calibrated total intensity is then $I = (E_A E_A^* \cdot g_A + E_B E_B^* \cdot g_B)/2$. For polarization data, the cross terms $Re(E_A^* E_B)$ and $Im(E_A^* E_B)$ must be multiplied by a gain factor $g_{AB} = \sqrt{g_A g_B}$.[1]

[1] These quantities are related to the Stokes parameters by equation 2.8

In practice, $(K/c)_i$ may change with parameters such as observing bandwidth, while G_i is expected to be more stable. Observations of a standard source are therefore used to determine this latter quantity. To obtain a gain factor g_i appropriate for each polarization at each observation, G_i (determined as described above), is coupled with $(K/c)_i$ as determined from pulsed noise observations using the current observing parameters. If the calibration observations used to determine $(K/c)_i$ for the current observing parameters are at a different bandwidth than the standard source calibration observations used to determine G_i, then the two quantities are combined by matching channels by frequency.

Note that the value of g_i is independent of the value of T_{CAL_i} which is actually used, and so this method may be used whether or not it is known, as long as the pulsed noise source is stable with time. If the value of T_{CAL} is not accurate, however, the individual values of G and T_{ANT} will not be accurate.

2.4.1 Practicalities

A noise source which is correlated between the two polarizations allows a determination of the instrumental phases in the system, as will be discussed in Section 2.5.3. This was true for most of our observations, allowing the standard calibrator noise signals to be used. For the 575-MHz system at Green Bank, independent noise sources are usually injected after the hybrid, so no measurement of instrumental phase between circular polarizations is possible. A single noise source was therefore coupled into the system at the feed, resulting in a correlated noise source, to allow measurement of the phases for each channel. The temperature of this source was, however, unknown. Values of T_{CAL_i} were chosen such that the antenna temperatures of the two polarizations were nearly equal, as is true when the standard calibration signal with known temperature is used. As noted above, these values do not affect the final gain calibration. For a few observations, this correlated calibration source was not available, so the standard pulsed noise source was used. In these cases, the observations were only included in the calculation if the antenna temperatures were nearly equal for all channels, as is expected. This also gave the most consistent gain calibration between channels.

Table 2.2 displays the standard sources used for each observing run and frequency, along with their fluxes in Janskys, the type of pulsed noise source used (correlated or standard), the observing system, and the rms of the antenna temperature ratio across the channels, which provides some estimate of the error in the resulting gain calibration of the data.

Gain Calibration Sources

Dates	Freq MHz	Source	Flux Jy	CAL Type	Observing System	Estimated Error(%)
1997 7/25-30	575	3C 48	30.9	C/S[a]	GBPP	15/10
		3C 286	22.0	C/S		15/5
1996 11/13-12/02	610	none[b]		C	GBPP	50
1995 1/29-31, 2/5-7	800	3C 48	24.4	S	CDRP-0	6,20
1995 2/3-5	800	none[c]		S	CDRP-0	–
1997 2/10-12, 4/26-30	820	3C 48	24.0	S	GBPP	6,5
1997 7/30-1	820	3C 48	24.0	C	GBPP	10
1997 7/31-8/1	820	3C 48	24.0	S	GBPP	5
1996 10/5,15	1410	none[b]			EBPP-a	–
1997 3/19-20, 3/23-4	1410	1345+12[d]			EBPP	7
1997 4/9-10	1410	1345+12	5.25	C	EBPP	7
		4C12.50				

[a]C-correlated CAL, S-standard independent linearly polarized CALs

[b]Calibration was achieved by assuming that the system temperatures of the two polarizations were equal.

[c]Calibration was achieved using K/c values

[d]used 4/9-10 calibration data

Table 2.2: Gain Calibration Sources are summarized for each observing date and frequency. The standard source and its associated flux in Jy are listed in columns three and four. The CAL type in column 5 is designated C if the injected CAL signal was correlated, and S if it was nominally uncorrelated (although for all but the 575-MHz data a small amount of correlation was introduced in the hybrid). The observing system is listed in column 6. An estimate in the error in the gain calibration is provided by the *rms* variation of the antenna temperature ratio about the mean, and is given in column 7.

2.5 Polarization Calibration

2.5.1 Theory

When taking polarization data, we are measuring radiation from orthogonal polarizations A and B, but the observed radiation will have been affected by passage through the telescope system. Following the formalism of McKinnon (1994), the measured radiation $E_A{}'$ and $E_B{}'$ relates to the intrinsic radiation E_A and E_B via

$$\begin{pmatrix} E_A{}' \\ E_B{}' \end{pmatrix} = \begin{pmatrix} T_{AA} & T_{AB} \\ T_{BA} & T_{BB} \end{pmatrix} \begin{pmatrix} E_A \\ E_B \end{pmatrix} \tag{2.6}$$

where the elements of this transmission matrix are

$$\mathbf{T} = g \begin{pmatrix} 1 & K_{AB}e^{i\theta_{AB}} \\ K_{BA}e^{i\theta_{BA}} & K_{BB}e^{i\theta_{BB}} \end{pmatrix}, \tag{2.7}$$

where g is the overall gain factor, $K_{BB}e^{i\theta_{BB}}$ describes the relative gain and phase between A and B, and the cross terms describe the coupling between the two polarizations. This matrix contains 7 independent parameters.

We now consider the effects of this transmission matrix on the intrinsic Stokes parameters, which are

$$\mathbf{S} = \begin{pmatrix} S_0 \\ S_1 \\ S_2 \\ S_3 \end{pmatrix} = \begin{pmatrix} E_A E_A^* + E_B E_B^* \\ E_A E_A^* - E_B E_B^* \\ 2Re(E_A E_B^*) \\ 2Im(E_A E_B^*) \end{pmatrix}. \tag{2.8}$$

When A and B correspond to linear polarizations X and Y this corresponds to $\mathbf{S}^T = (I, Q, U, V) = (I, P\cos(2\chi), P\sin(2\chi), V)$, whereas for circular polarizations L and R this is $(I, V, Q, U) = (I, V, P\cos(2\chi), P\sin(2\chi))$, where the linear polarization is described by amplitude P and position angle χ with $Pe^{i2\chi} = Q + iU$. Positive V is associated with left-handed circular polarization.

Apart from the overall and relative gain factors g and K_{BB}, which can be removed using gain calibration, the dominant effect is the relative phase between A and B introduced by the telescope. In addition to this phase angle, there are telescope parameters K_{BA}, θ_{BA}, K_{AB}, and θ_{AB} which describe the way in which intrinsic polarization B is detected in measured polarization A and vice versa. For known telescope parameters, the instrumental effect on the intrinsic Stokes parameters $\mathbf{S}$ is given by

$$\mathbf{S}''(\beta) = \mathbf{M} \cdot \mathbf{R}(2\beta) \cdot \mathbf{S}, \tag{2.9}$$

where $\mathbf{M} = \frac{g^2}{2}\mathbf{M_0}$ is the Mueller matrix and $\mathbf{M_0}$ is shown in equation 2.10 on page 47.

The matrix $\mathbf{R}(2\beta)$ is the rotation matrix used to rotate the Q and U components by 2β, which is the orientation angle of the feed relative to the source. In the circular polarization basis, this matrix is

$$\mathbf{R}(2\beta) = \begin{pmatrix} 1 & 0 & 0 & 0 \\ 0 & 1 & 0 & 0 \\ 0 & 0 & \cos(2\beta) & \sin(2\beta) \\ 0 & 0 & -\sin(2\beta) & \cos(2\beta) \end{pmatrix}. \tag{2.11}$$

If A and B are truly orthogonal, then this implies that $K_{BA} = K_{AB} = 0$, and the instrumental effects are described by

$$\mathbf{M} = \frac{g^2}{2}\begin{pmatrix} 1+K_{BB}^2 & 1-K_{BB}^2 & 0 & 0 \\ 1-K_{BB}^2 & 1+K_{BB}^2 & 0 & 0 \\ 0 & 0 & 2K_{BB}\cos(\theta_{BB}) & 2K_{BB}\sin(\theta_{BB}) \\ 0 & 0 & -2K_{BB}\sin(\theta_{BB}) & 2K_{BB}\cos(\theta_{BB}) \end{pmatrix},$$

where $g = K_{BB} = 1$ holds for previously gain-calibrated data.

If A and B are circular polarizations, the relative phase angle θ_{BB} causes a rotation between Stokes parameters Q and U, and is thus simply a rotation of the position angle. If we are using the linear polarization basis, then this angle causes a rotation between Stokes parameters U and V. This completely corrupts observations of the polarization of the source, and must be carefully removed. In the non-orthogonal case, the instrumental terms K_{BA}, θ_{BA}, K_{AB}, and θ_{AB} affect all of the Stokes parameters, and their interdependence is considerably more complicated.

2.5.1.1 Circular Basis

In the basis of circular polarizations L and R, it is physically meaningful to write the transmission matrix $\mathbf{T}$ as

$$\mathbf{T} = \begin{pmatrix} \dfrac{1}{(1+\epsilon_L^2)^{1/2}} & \dfrac{\epsilon_L e^{i\theta_L}}{(1+\epsilon_L^2)^{1/2}} \\ \dfrac{\epsilon_R e^{-i\theta_R}}{(1+\epsilon_R^2)^{1/2}} & \dfrac{1}{(1+\epsilon_R^2)^{1/2}} \end{pmatrix}, \tag{2.12}$$

assuming that the relative gain calibration has been applied, and that the relative instrumental phase between L and R will be dealt with separately. In this case

$$\begin{pmatrix} 1+K_{BB}^2+K_{AB}^2+K_{BA}^2 & 1-K_{BB}^2-K_{AB}^2+K_{BA}^2 & 2(K_{AB}\cos(\theta_{AB})+ & 2(K_{AB}\sin(\theta_{AB})+ \\ & & K_{BA}K_{BB}\cos(\theta_{BB}-\theta_{BA})) & K_{BA}K_{BB}\sin(\theta_{BB}-\theta_{BA})) \\ 1-K_{BB}^2+K_{AB}^2-K_{BA}^2 & 1+K_{BB}^2-K_{AB}^2-K_{BA}^2 & 2(K_{AB}\cos(\theta_{AB})- & K_{AB}\sin(\theta_{AB}))+ \\ & & K_{BA}K_{BB}\cos(\theta_{BA}-\theta_{BB})) & K_{BA}K_{BB}\sin(\theta_{BA}-\theta_{BB})) \\ 2(K_{BA}\cos(\theta_{BA})+ & 2(K_{BA}\cos(\theta_{BA})- & 2(K_{BB}\cos(\theta_{BB})+ & 2(K_{BB}\sin(\theta_{BB})+ \\ K_{AB}K_{BB}\cos(\theta_{AB}-\theta_{BB})) & K_{AB}K_{BB}\cos(\theta_{AB}-\theta_{BB})) & K_{AB}K_{BA}\cos(\theta_{AB}-\theta_{BA})) & K_{AB}K_{BA}\sin(\theta_{AB}-\theta_{BA})) \\ 2(-K_{BA}\sin(\theta_{BA})+ & 2(-K_{BA}\sin(\theta_{BA})- & 2(-K_{BB}\sin(\theta_{BB})+ & 2(K_{BB}\cos(\theta_{BB})- \\ K_{AB}K_{BB}\sin(\theta_{AB}-\theta_{BB})) & K_{AB}K_{BB}\sin(\theta_{AB}-\theta_{BB})) & K_{AB}K_{BA}\sin(\theta_{AB}-\theta_{BA})) & K_{AB}K_{BA}\cos(\theta_{AB}-\theta_{BA})) \end{pmatrix} \tag{2.10}$$

the nominally orthogonal circularly polarized response of the telescope is actually elliptically polarized, with axial ratios $\rho_i = (1-\epsilon_i)/(1+\epsilon_i)$, and position angles of the major axes $\tau_i = \theta_i/2$. See equation A.5 of Stinebring (Stinebring 1982) for the complete Mueller matrix resulting from this definition.

In practice, $\epsilon_i << 1$, so the complex leakage factors $\boldsymbol{\epsilon_L} = \epsilon_L e^{i\theta_L}$ $\boldsymbol{\epsilon_R} = \epsilon_R e^{i\theta_R}$ correspond directly to $K_{LR}e^{i\theta_{LR}}$ and $K_{RL}e^{i(\theta_{RL}-\theta_{RR})}$ in the earlier formulation.

By defining the sum and difference vectors,

$$\begin{aligned} \boldsymbol{\sigma} = \sigma e^{i\psi_\sigma} &= \boldsymbol{\epsilon_L} + \boldsymbol{\epsilon_R} = \epsilon_L e^{i\theta_L} + \epsilon_R e^{-i\theta_R} \\ \boldsymbol{\delta} = \delta e^{i\psi_\delta} &= \boldsymbol{\epsilon_L} - \boldsymbol{\epsilon_R} = \epsilon_L e^{i\theta_L} - \epsilon_R e^{-i\theta_R} \end{aligned} \tag{2.13}$$

and neglecting terms of ϵ_i^2, the Mueller matrix becomes

$$\mathbf{M} = \begin{pmatrix} 1 & 0 & \sigma\cos(\psi_\sigma) & \sigma\sin(\psi_\sigma) \\ 0 & 1 & \delta\cos(\psi_\delta) & \delta\sin(\psi_\delta) \\ \sigma\cos(\psi_\sigma) & -\delta\cos(\psi_\delta) & 1 & 0 \\ \sigma\sin(\psi_\sigma) & -\delta\sin(\psi_\delta) & 0 & 1 \end{pmatrix}.$$

Even if the telescope response is elliptically rather than circularly polarized, they may be orthogonal to one another if $\epsilon_L = \epsilon_R$ and $\theta_L = \theta_R + \pi$, implying $\sigma = 0$.

We have separated out the effects of the relative phase $\psi = \theta_{RR}$ between the polarizations L and R, so we model the measured Stokes by

$$\begin{aligned} \mathbf{S}''(\beta) &= \mathbf{R}(\psi)\cdot\mathbf{M}\cdot\mathbf{R}(2\beta)\cdot\mathbf{S} \\ &= \begin{pmatrix} I + P\sigma\cos(\phi-\psi_\sigma) \\ P\cos(\phi-\psi) + I\sigma\cos(\psi_\sigma+\psi) - V\delta\cos(\psi_\delta+\psi) \\ P\sin(\phi-\psi) + I\sigma\sin(\psi_\sigma+\psi) - V\delta\sin(\psi_\delta+\psi) \\ V + P\delta\cos(\phi-\psi_\delta) \end{pmatrix}, \end{aligned} \tag{2.14}$$

where $\phi = 2(\chi - \beta)$.

Thus the Stokes parameters will vary sinusoidally with the angle β describing the relative orientations of the feed and the source position angle.

2.5.2 Calibration Procedure

In what follows, we assume that the gain calibration has been carried out using the standard method described in section 2.4. We may therefore set the overall and relative gain parameters g and K_{BB} to 1 before proceeding further. To determine the other telescope parameters, we must observe a source for which the Stokes parameters

are known. Equation 2.14 shows that the instrumental polarization parameters will determine the sinusoidal variations of the Stokes parameters with feed angle β. For a source with a single constant position angle, it is necessary to observe the source for many different rotation angles β of the feed, in order to obtain measurements at many effective position angles of the polarized source. For a telescope with an alt-azimuth mount, this is achieved simply by tracking the source across the sky, since the orientation of the feed relative to the source changes during the observation (cf. Stinebring 1982). For a telescope with a polar mount, the relative positions of the feed and the source do not change during tracking, so the feed angle must be intentionally rotated (McKinnon 1994). For N such observations of the measured Stokes $\mathbf{S}'$, we may fit for the n_p parameters of the Mueller matrix $\mathbf{M}$ by comparing these with the model Stokes $\mathbf{S}''$, and minimizing an averaged χ^2 defined by

$$\chi^2 = \frac{1}{4(N - n_p - 1)} \sum_{i=0}^{3} \sum_{j=0}^{N-1} (S_{ij}{}' - S_{ij}{}'')^2. \tag{2.15}$$

In the case of a pulsar, however, we can obtain a measurement of the Stokes parameters at many phases across the pulse. Then the position angle changes automatically across the pulse according to the sweep of the position angle of the pulsar. This approach has been taken by Stinebring (1982) and Xilouris (1991). Even if the position angle changes only modestly across the pulse, a small number of feed rotation angles will adequately sample the total range of effective position angles. Thus, given a pulsar for which the Stokes parameters are known, we can perform the least-squares fit discussed above. In practice, this is complicated by the fact that pulsars scintillate due to the effects of the interstellar medium, and so the total intensity I is not constant in time. Following Stinebring (1982), we note that the quantity $I_{const} = [I^2 - (Q^2 + U^2 + V^2)]^{1/2}$ is a constant under the transformation of the Mueller matrix, so it may be used to correctly normalize all measured Stokes profiles prior to fitting for instrumental parameters.

Once the polarization parameters of the telescope are determined, the Mueller matrix $\mathbf{M}$ is fully known, and the true measured Stokes parameters $\mathbf{S_{cal}}$ of a source of unknown polarization may be determined using simple matrix inversion:

$$\mathbf{S_{cal}}(\beta) = \mathbf{R}(-2\beta) \cdot \mathbf{M^{-1}} \cdot \mathbf{R}(-\theta_{BB}) \cdot \mathbf{S}' \tag{2.16}$$

where the relative phase angle θ_{BB} has been separated from the Mueller matrix as was done explicitly above for the circular basis.

2.5.3 Application to Circular Polarization data

If the relative instrumental phase introduced between the two circular polarizations varies significantly across the bandwidth of the system, then depolarization of the polarization profile will result when the data are averaged, unless this instrumental effect has been first removed.

At Effelsberg, a single linearly polarized pulsed noise source is injected prior to the hybrid. Given knowledge of the intrinsic position angle of this calibrator signal, the instrumental rotation ($\psi = \theta_{RR}$) may be determined by measuring the position angle from the Q and U components of the pulsed noise signal for each channel. In practice, we do not know the intrinsic position angle of the calibrator, but θ_{RR} varies substantially between channels for the BPP systems, and so this measurement allows the relative instrumental phase between channels to be determined. This measurement may then be used to remove the instrumental phase from all the data. This was done for the 1997 March and April data, but was not possible for the 1996 October data. The same is true for the non-standard correlated calibrator signal which was injected into the 575-MHz system at Green Bank (cf. Section 2.4.1).

For the 800-MHz system at Green Bank, independent linearly polarized noise sources are injected prior to the hybrid. If they had equal amplitudes, any pulsed noise signal visible in the polarization cross terms would be introduced by the hybrid. If the amplitudes are not equal, then there is a net linear polarization in the signal. In either case, measurement of the pulsed noise signal in the two cross terms again allows measurement of the instrumental phase. Since most of the 820-MHz data were obtained during standard timing runs, these standard noise sources were used. For a brief period of time in 1997 July, a correlated noise signal was introduced as for the 575-MHz system, to improve the measurement of the relative phase. A comparison of the measurement using the two different CAL signals revealed that for some channels, the results differed systematically by $30 - 40°$. These were exactly the channels for which the instrumental phase resulted in very little signal in one of Q or U. In these cases, the more weakly correlated standard CAL provided insufficient signal for the measurement. As a result, the measurement of the more strongly correlated signal was applied to all the data for that epoch. This procedure was confirmed by inspecting the resulting relative PPA values for PSR B1937+21 after application of the two possibilities. It is possible that similar problems in measurements of the instrumental phase were present for the other 1997 820-MHz data.

For the 1995 January/February data taken in the circular polarization basis, no attempt has been made to remove the relative instrumental phases across the 16 channels of CDRP-0.

2.5.3.1 1410-MHz EBPP data

In order to determine the remaining instrumental parameters, polarization measurements are made of a pulsar with known Stokes parameters at a variety of feed angles. PSR B1929+10 was used for this purpose. To use this object, we needed to know its intrinsic polarization properties. At 1410 MHz we obtained polarization profiles from both Stinebring (1982), who kindly sent us his thesis data, and from Gould & Lyne (1997).[2] These were interpolated to the resolution of our data. The data were gain-calibrated, and the instrumental phase was removed as described above. The model Stokes parameters for this object were compared with the data for all points in the region where the model exceeded a specified threshold (usually 10% of the peak), in a global fit using equations 2.14 and 2.15. The data were normalized as described in Section 2.5.2, after which a simple grid search algorithm determined the following parameters: the offset in polarization position angle between the data and model profiles, the gain factor required to match the data to the model profile, and the Mueller matrix parameters $\delta, \psi_\delta, \sigma$, and ψ_σ. These final parameters were used to invert the Mueller matrix for application to the data for the remaining pulsars. Similar results were obtained in fits using both model profiles. A separate fit was done for data taken on each day of observations. The magnitudes of δ and σ are similar for each day, but the phases ψ_δ and ψ_σ were not constant. The results from the appropriate day were therefore applied to all pulsar data, although the signal to noise of the PSR B1929+10 data for the 1997 April 9/10 was lower, resulting in less certainty about the instrumental calibration.

It is apparent from equation 2.14 that the measured Stokes parameters will vary sinusoidally with the angle β describing the relative orientations of the feed and source PPA, with vertical offsets equal to the true values of the Stokes parameters.

Figure 2.2 displays the B1929+10 Stokes parameters (I', Q', U', V') for a single channel of 1410-MHz EBPP data from a single day, averaged over the center of the gain-calibrated pulse profile, normalized by $I'_{const} = [I'^2 - (Q'^2 + U'^2 + V'^2)]^{1/2}$, and plotted against β, which includes both the feed angle and the parallactic angle correction. The expected sinusoidal variations with β are visible. The top 3 panels of Figure 2.3 display, for all channels, the results of a fit which included only the instrumental parameters δ and ψ_δ, setting $\sigma = 0$. The dotted lines in Figure 2.2 result from applying the Mueller matrix corresponding to these parameters to the average Stokes model. The solid lines result from applying results of a fit which also

[2]Obtained from the data base of published profiles maintained by the European Pulsar Network, available at: http://www.mpifr-bonn.mpg.de/pulsar/data/

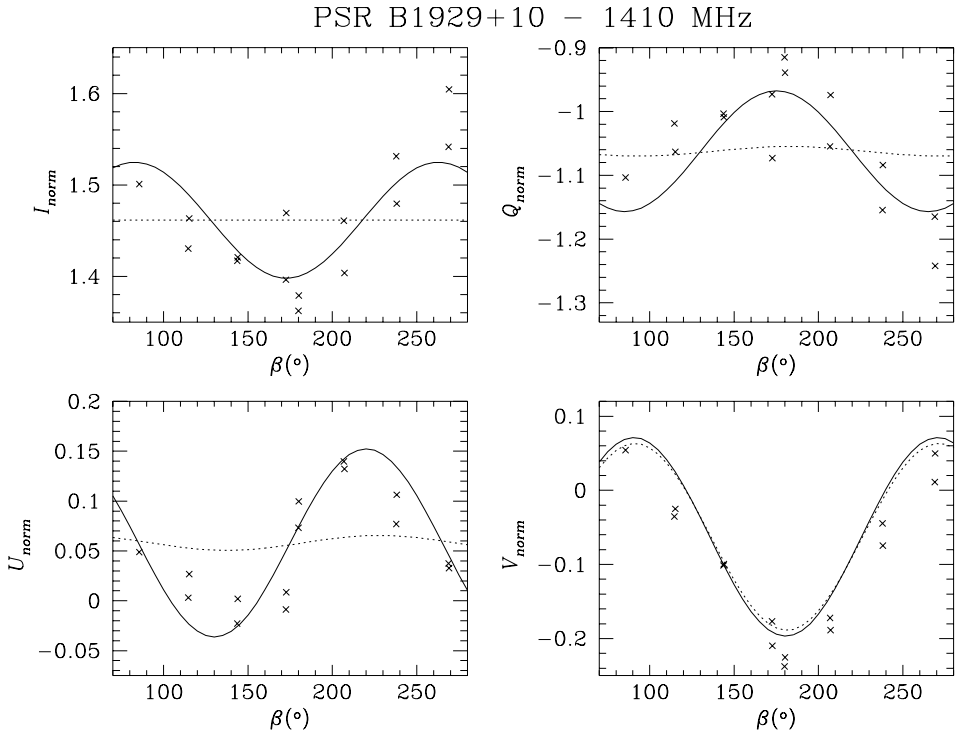

Fig. 2.2.— Stokes vs. β for PSR B1929+10 at 1410 MHz. Gain-calibrated Stokes parameters were produced for the PSR B1929+10 data which were taken with the EBPP on 1997 March 24. The average values for a region centered on the pulse (for which the model Stokes intensity exceeded $I/I_{max} = 0.1$) were determined. These were normalized by $I_{const} = [I^2 - (Q^2 + U^2 + V^2)]^{1/2}$. The results are plotted for a single channel against the feed + parallactic angle β. The dotted and solid lines result from applying an instrumental correction to the average model Stokes. The instrumental parameters determined in a fit for δ and ψ_δ, shown in the top panels of Figure 2.3, were used to produce the dotted lines. The solid lines result from using the results of a fit which also included σ and ψ_σ, which are shown in the bottom panels of Figure 2.3.

included σ and ψ_σ to the model Stokes. The parameters of this fit are displayed in the bottom 5 panels of Figure 2.3. Figure 2.4 displays the same averaged Stokes parameters for data which has been corrected for instrumental effects using the inverse Mueller matrix for the displayed parameters.

In all these figures, the sign of V has been changed in our data to match the published polarization profiles. Although such a sign change in this case could be due to an error in gain calibration, the original sign of the sense-reversing V in our observations of PSR B0355+54 also disagreed with the published literature (Gould & Lyne 1997[2], von Hoensbroech & Xilouris 1997b[3]). Gain calibration errors could not

[3]The sign of V in the 1.7 GHz profile is unclear, but the sense of V in profiles at other frequencies matches that of the other authors at lower frequencies.

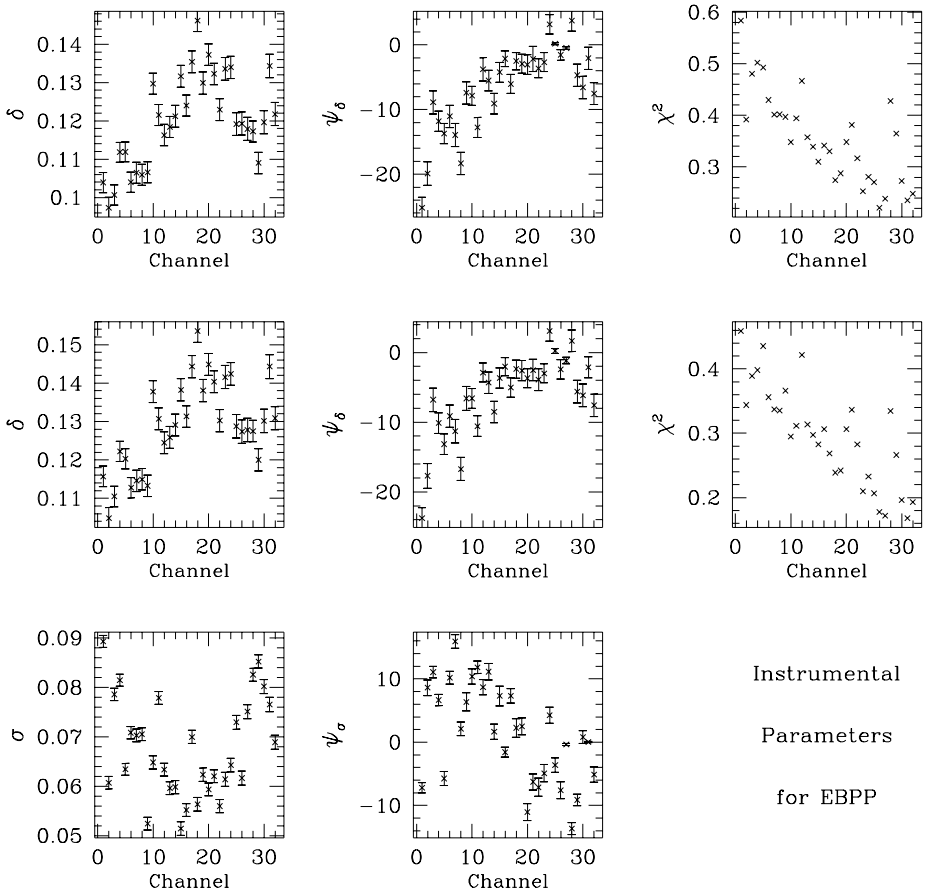

Fig. 2.3.— Instrumental Polarization Parameters for Effelsberg. The top three panels display the values for each channel of the instrumental parameters determined in a fit, along with the χ^2 of the fit. The data used in the fit were the same as that which were used to generate the average quantities displayed in Figure 2.2. The telescope response was assumed to be orthogonal, so only δ and ψ_δ were included in the fit. The bottom five panels display the results for a fit which also included the orthogonality parameters σ and ψ_σ.

have this effect. If the polarizations L and R had been mis-identified at the telescope, then the direction of the PPA curve would also be reversed relative to the published results, which is not the case. This correction has been applied to all 1410-MHz EBPP data. As further confirmation that this is the appropriate action, we note that the signs of V for most of the millisecond pulsars are consistent across all observed frequencies after this correction has been made. The source of this sign reversal of V remains unexplained. No similar sign correction is required for the 820-MHz or 575-MHz data. A similar sign reversal may affect the millisecond pulsar polarization data published in Xilouris *et al.* (1988).

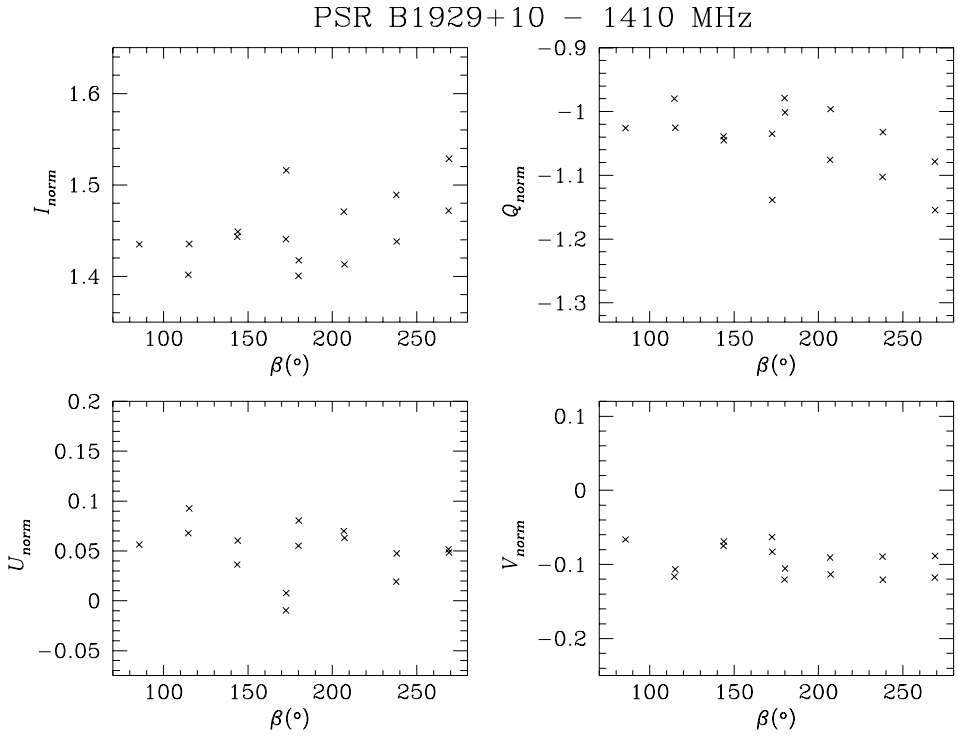

Fig. 2.4.— Corrected Stokes vs. β for PSR B1929+10. The inverse Mueller matrix resulting from the full fit for instrumental parameters shown in Figure 2.3 was applied to the gain calibrated Stokes parameters for the same data as that used to generate Figure 2.2. The average values for the central region were determined, normalized by I_{const}, and plotted against β, as before. The sinusoidal variations have been largely removed.

2.5.3.2 575-MHz GBPP data

It is apparent from equation 2.14 that for $\sigma << 1$,

$$\frac{V'}{P'} = \frac{V}{P} + \delta \cos(2(\chi - \beta) - \psi_\delta). \tag{2.17}$$

The measured value of V'/P' will vary sinusoidally with the angle β, with an offset of the true value of V/P.

The first panel of Figure 2.5 displays V'/P' for the 575-MHz PSR B1929+10 Stokes data for a single day, plotted against β. The data were averaged over the center of the gain-calibrated pulse profile, and over sets of 8 channels. In the GBPP, a separate LO is used for each block of 8 channels, so instrumental parameters are expected to be most similar within a block. Each set of 8 channels is represented by a different symbol. The second panel of Figure 2.5 displays the same quantities for a different day of data. The solid lines result from applying the instrumental parameters $\delta = 0.05$, $\psi_\delta = -60°$ to an estimate of the average model Stokes values derived from the offsets

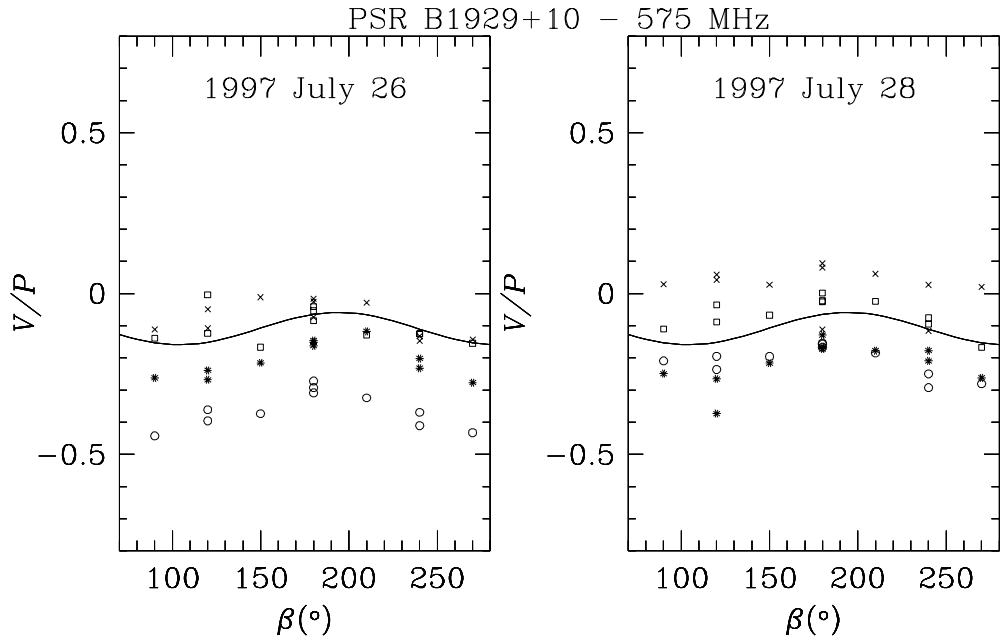

Fig. 2.5.— V/P vs. Feed Angle β for PSR B1929+10 at 575 MHz. The 575-MHz Stokes parameters of PSR B1929+10, averaged in 4 sets of 8 channels, were averaged over the central region of the pulse. The quantity V/P is plotted against feed angle β for each set of channels for 2 separate days (1997 July 26/28). Each set of channels is marked with a different symbol. Note the difference in the results of gain calibration for each set of channels. The solid lines result from applying the instrumental parameters $\delta = 0.05$, $\psi_\delta = -60°$ to the model Stokes.

of the sinusoids in the data for 1997 July 28. Note that there are significant difficulties with the gain calibration of this data, with systematic effects between the channel groups of order $\pm 10\%$. Despite difficulties with the vertical offset, the amplitude and phase of the instrumental effects can be estimated. A correction for these values of δ and ψ_δ has been applied to all 575-MHz data. The corresponding plots produced from the corrected data reveal that the sinusoidal variations are correctly removed. Plots of all four normalized Stokes parameters reveal that $\sigma \lesssim 5\%$. No correction for $\sigma \neq 0$ has been made.

2.5.3.3 820-MHz GBPP data

Most of the 820-MHz GBPP data were obtained during standard pulsar timing runs, with the GBPP obtaining polarimetry using the same schedule as the Spectral Processor. As a result, extensive rotations of the feed were not possible.

Observations of PSR B1929+10 at a single feed angle (1997 February) imply that the instrumental effects could be of order 10-20%, but the fits are poorly constrained in this instance. As a result, no correction for instrumental polarization was applied

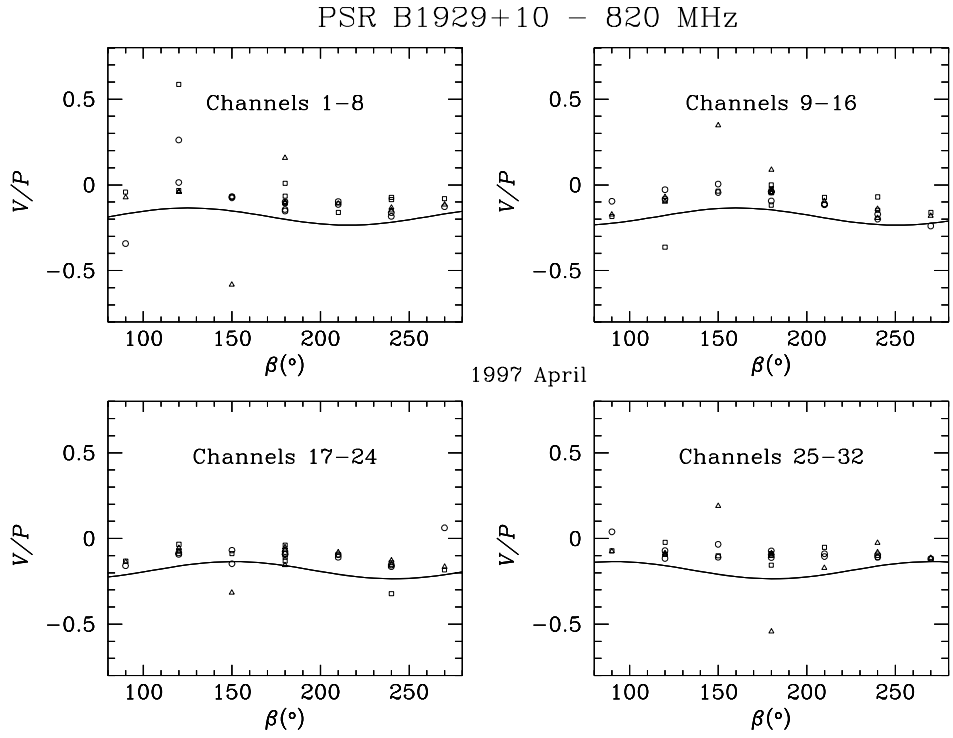

Fig. 2.6.— V/P vs. β at 820 MHz for 1997 April. The 820-MHz Stokes parameters of PSR B1929+10, averaged in 4 sets of 8 channels, were averaged over the central region of the pulse. The quantity V/P is plotted against feed angle β for each set of channels for three separate days (1997 April 28-30). Each symbol represents a different observing date. The solid lines result from applying the instrumental parameters $\delta = 0.05$, $\psi_\delta = 40, -30, -10, 110°$ to the model Stokes. The different values of ψ_δ are required to account for the different sinusoidal phase for each set of 8 channels.

to this data.

During the several days of observing in 1997 April, observations of PSR B1929+21 with feed angle rotation were taken on three days. The four panels of Figure 2.6 display V'/P' for the 820-MHz PSR B1929+10 Stokes data, plotted against feed angle β. The data have been averaged over the center of the gain-calibrated pulse profile, and over the four sets of 8 channels, and plotted against β. Each symbol represents a different day of observations. The solid lines result from applying the instrumental parameters $\delta = 0.05$, $\psi_\delta = 40, -30, -10$ and $110°$ to the average model Stokes, which at this radio frequency were obtained from Stinebring (1982). Plots of all four Stokes parameters limit sigma to $\approx 5\%$. The 1997 April GBPP data were corrected for these instrumental parameters, setting $\sigma = 0$. The corresponding plots of V/P for the corrected data show much less variation with feed angle β.

In 1997 July, a single set of observations of PSR B1929+10 with feed rotation is

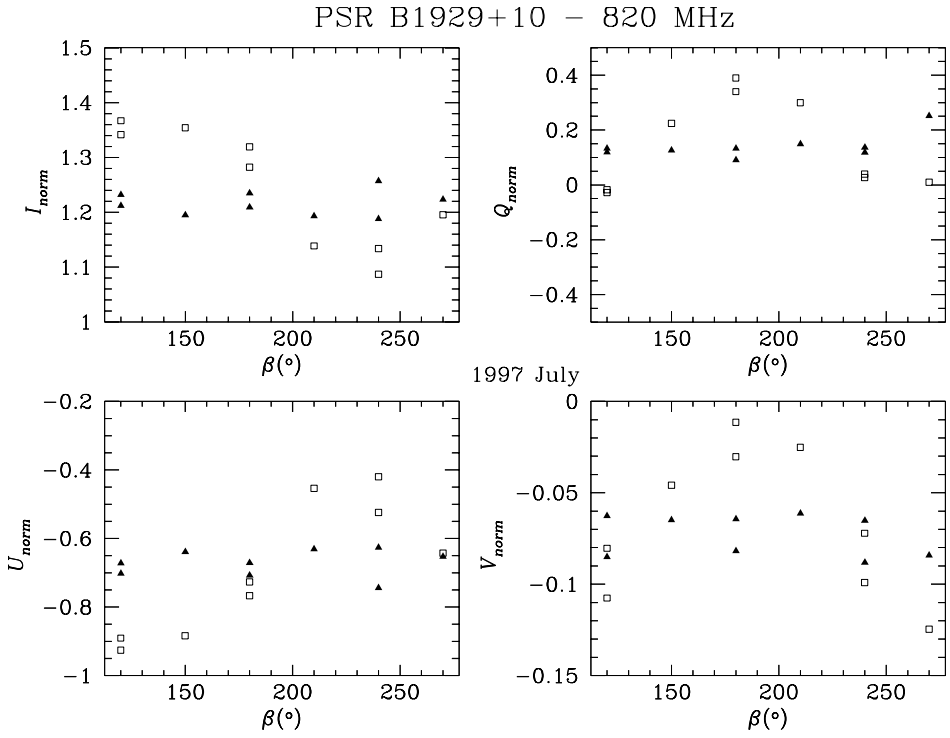

Fig. 2.7.— Stokes vs. β for PSR B1929+10 at 820 MHz for 1997 July. The normalized Stokes parameters, averaged over the center of the pulse, and over all channels, are displayed against feed angle β for the PSR B1929+10 data which were taken with the GBPP on 1997 July 31. No polarization calibration has been applied to the data represented by the open squares. The correction matrix $\mathbf{M^{-1}}$ for the instrumental parameters $\delta = 0.07$, $\psi_\delta = -70°, -80°, -90°, -100°$, $\sigma = 0.2$, $\psi_\sigma = -6°$ has been applied to the data from which the values for the filled triangles were determined. The sinusoidal variation has been largely eliminated.

available. The normalized Stokes parameters, averaged over the central region and all channels, are displayed against β in Figure 2.7. The open squares represent data to which no instrumental corrections have been applied. The sinusoidal amplitude in all Stokes parameters is quite large, indicating $\sigma \sim 0.2$. If σ had been this large in the 1997 April data, it would have been clearly visible. The filled triangles represent data to which an instrumental correction has been applied, using the parameters $\delta = 0.07$, $\psi_\delta = -70, -80, -90, -100°$, $\sigma = 0.2$, and $\psi_\sigma = -6°$. Inspection of blocks of eight channels revealed that similar parameters were appropriate for all. These same parameters were applied to all 1997 July 820-MHz data.

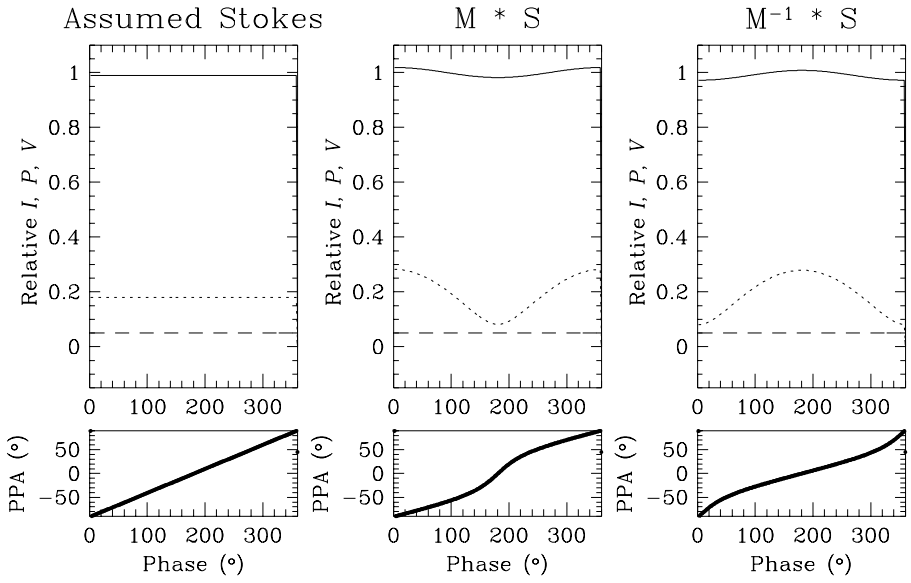

Fig. 2.8.— Effect of $\sigma \neq 0$ on PPA. For Stokes parameters with low linear polarization P, such are displayed in the first panel, even modest values of the instrumental parameter σ have a significant effect on the PPA. In the second and third panels, the forward and inverse Mueller transformations for $\delta = 0$, $\sigma = 0.1$, and $\phi_\sigma = 0$ have been applied to these Stokes. The transformation of the PPA curve is significantly non-linear.

2.5.4 The effects of $\sigma \neq 0$ on PPA

The effects of even modest values of σ on the PPA curve are small, if the linearly polarized fraction is high ($P \sim I$). If the linearly polarized fraction is small, then even $\sigma \sim 0.1$ has a significant effect on the PPA curve. The first panel of Figure 2.8 displays Stokes parameters in which the PPA curve is assumed to vary linearly across the pulse. The linearly polarized fraction is assumed to be $P/I = 0.2$, with $V = 0$. The results of applying a Mueller matrix with $\sigma = 0.1$, $\psi_\sigma = 0$ ($\delta = 0$ has been assumed for clarity) are displayed in the second panel. The expected sinusoidal variations of I and P are visible, and the instrumental effect results in a non-linear transformation of the PPA, with the location of the steepest portion of the new PPA curve depending on ψ_σ. The third panel displays the results of applying the inverse Mueller transformation to the original Stokes. This mimics the effect of an erroneous correction for $\sigma \neq 0$. Again, the PPA curve is distorted in a non-linear fashion. In light of these effects, one must be careful in interpreting the shape of the PPA curve in objects with very low linear polarization P.

2.5.5 Application to Linear Polarization data

2.5.5.1 Application to 140′ 800-MHz Data

Since the circular polarizations at 800 MHz on the 140′ telescope are produced by sampling of linear polarizations with subsequent mixing in a hybrid, the cross terms K_{LR} and K_{RL} are likely to be more important than the cross terms K_{xy} and K_{yx} for the linear polarizations. Thus linear polarizations were used for the first experiment. This has the disadvantage that the relative phase angle θ_{yy} causes a rotation between U and V, instead of the rotation between Q and U which is the principal effect of θ_{RR}, and is simply a rotation of position angle.

Gain calibration of all data discussed below was done using observations of the source 3C 48. The telescope polarization parameters were determined in two ways. First, by measuring at many feed angles the Stokes parameters of the standard source 3C 286, and second, by measuring the Stokes parameters of the well-studied pulsar B1929+10.

We determined the measured Stokes at several positions of the feed for 3C 286, which has a linear polarization of 9%. This was done through on and off source pulsed CAL measurements. Following McKinnon (1994), when $K_{yy} \sim 1.0$ and $S_1/S_0 << 1.0$, the quantity $f = S_1'/S_0' = Q/I$ reduces to

$$f(\beta) \sim b + m cos[2(\beta - \chi)], \tag{2.18}$$

where the percent linear polarization is given by the amplitude m of the sinusoid, and the intrinsic position angle is given by the phase χ. The offset $b \sim (1-K_{yy}^2)/(1+K_{yy}^2)$ should be zero for correctly gain calibrated data, since then $K_{yy} = 1.0$. Our data correctly displays the results of the 9% linear polarization of this object.

Using the fitted values for the intrinsic polarization of 3C 286, which has virtually no circular polarization, the intrinsic Stokes parameters are given by

$$\mathbf{S} = I \begin{pmatrix} 1 \\ m\cos(2\chi) \\ m\sin(2\chi) \\ 0 \end{pmatrix}. \tag{2.19}$$

These can be used to fit for the parameters defining the elements of the Mueller matrix, using the same methods discussed earlier. The values of K_{xy} and K_{yx} determined in this fit represent cross-coupling of at most a few percent.

We also observed the pulsar B1929+10 at a few feed angles, and fit for the PPA offset and the instrumental parameter θ_{yy} using data at a single feed angle. The

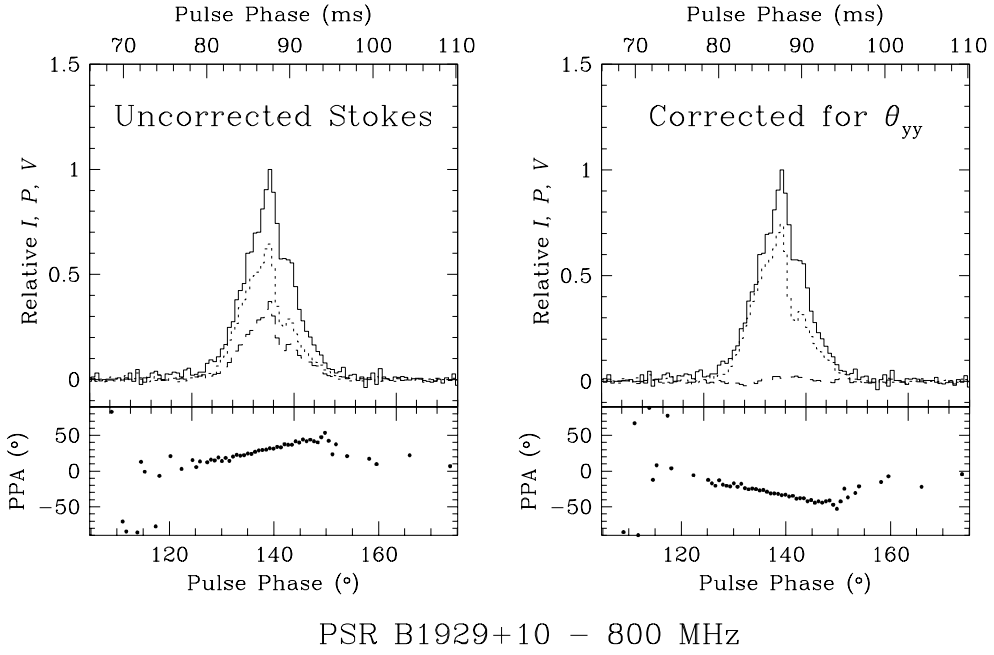

Fig. 2.9.— The effects of θ_{yy} on PSR B1929+10. The first panel displays gain-calibrated polarization data for a single channel to which no instrumental correction has been applied. The second panel displays the data after a correction for $\theta_{yy} \sim 145°$ has been applied.

results were largely consistent for data taken with each feed angle. The θ_{yy} values determined in these fits also agreed with the results for 3C 286, to within the errors.

The first panel of Figure 2.9 displays the gain-calibrated polarization data for PSR B1929+10. No instrumental correction has been applied. The second panel displays the results correcting for θ_{yy} as determined in a fit to another PSR B1929+10 data scan. This now compares favourably with the model Stokes obtained from Stinebring (1982).

An instrumental correction was applied to all of the data, using the results of the fits for θ_{yy} from PSR B1929+10, as this was available for both the 1997 January and 1997 February observations, whereas the 3C 286 calibration was available for only one of these.

2.5.5.2 Application to 85-3 data

The instrumental phase θ_{yy} introduced between the X and Y polarizations is also the dominant instrumental effect for the 610-MHz data presented here.

As in the case of circular polarizations, one measure of this angle θ^c_{yy} is given by the correlated pulsed CAL signal which can be injected into the signal path. The amount of pulsed signal which appears in the polarization cross terms is governed by

Polarization Calibration Summary

Dates	Freq MHz	δ	ψ_δ °	σ	ψ_σ °
1997 7/25-30	575	0.05	-60	0.	–
1995 2/3-5[a]	800	0.	–	0.	–
1997 2/10-12[a]	820	0.	–	0.	–
1997 4/26-30	820	0.05	$40, -30, 10, 110$	0.	–
1997 7/30-8/1	820	0.07	$-70, -80, -90, -100$	0.2	-6
1996 10/5,15[b]	1410	0.	–	0.	–
1997 3/19-20, 3/23-4	1410	~ 0.12	various	~ 0.07	various
1997 4/9-10	1410	~ 0.12	various	~ 0.07	various

Dates	Freq MHz	θ_{yy} °
1995 1/29-31	800	135 to 145
1995 2/5-7	800	-90 to -60

[a] none available - standard timing run

[b] none available

Table 2.3: Polarization Calibration Summary. For each observing session, the observing frequency is listed, followed by the polarization parameters used to correct the data for instrumental effects. See text for details.

the value of this phase angle for the signal path *following* the CAL. This is sufficient in the case of circular polarizations, where only the relative value between channels is important. In this case, however, we need to know the true value. To measure this phase angle for the entire signal path, observations of the Vela pulsar were used to fit for both θ^d_{yy} and the rotation in position angle due to the atmosphere, as was done for PSR B1929+21 in the previous section. The phase angle due to the signal path *before* the CAL signal is injected was found to be relatively constant, over a large range of dates. This

$$\Delta\theta_{yy} = \theta^d_{yy} - \theta^c_{yy}$$

was then added to the value of θ^c_{yy} determined for observations of the Crab pulsar.

Table 2.3 contains a summary of instrumental parameters used to apply corrections to the GBPP and EBPP data. For each date and frequency, the values of δ, ψ_δ, σ, and ψ_σ are tabulated for the observations taken using the circular basis, while θ_{yy} is tabulated for the linear polarization basis.

2.6 Data Reduction

The calibration procedures described in sections 2.4 and 2.5 may be applied to each channel of the BPP, for each scan. In principle the resulting polarization profiles may be averaged to improve signal to noise once any parallactic angle differences have been removed. In practice this is complicated by the rotation measure RM as defined in equation 1.18, as well as any remaining systematic PPA variations due to instrumental effects. Addition of two polarization profiles with improperly aligned position angles results in depolarization of the summed profile. Specifically, if two profiles with linear polarization P_0 are combined, then the linear polarization of the average P is

$$\frac{P}{P_0} = \frac{1 + \cos(\Delta\chi)}{2} \tag{2.20}$$

where $\Delta\chi$ is the rotation in position angle between the two profiles. For smooth variations of PPA resulting in a total change $\Delta\chi$ across our observing bandwidth, the effect will be smaller than that indicated by equation 2.20.

The rotation measure of the ionosphere is typically $1 - 10$ rad m^{-1}. The variation is dominated by a diurnal effect, but solar flux and magnetic field variations also play a role. For a rotation measure of 10, and a bandwidth of 30 MHz, the change in polarization position angle across the band is then $\Delta\psi = 1°$ at 1410 MHz, 6° at 820 MHz, and 16° at 575 MHz. If the rotation measure changes by $\Delta RM = 9$, then the change in position angle at the center of our band is 23° at 1410 MHz, 69° at 820 MHz, and 140° at 575 MHz. This affects not only the summing over the frequency channels, but also the averaging of data taken at different times.

In addition to the RM of the ionosphere, the pulsar has a rotation measure due to propagation through the interstellar medium. Although the magnetic field is weak, the long propagation path results in measurable effects. For these objects, the true interstellar rotation measure is unknown, and so we must determine if a large RM is present.

In order to assess these effects, average polarization profiles (1-3 per pulsar observation) were originally produced with $RM = 0$ and the effects of θ_{RR} removed. These were added together to create profiles with a reasonable S/N. The PPA offset between these profiles was determined, by fitting using one of the profiles as a template. These angle offsets were then removed from polarization profiles for all frequency channels, which were added, and a PPA offset was determined for each channel. Finally, a least-squares fit was performed to determine the RM, assuming that the instrumental phases have been correctly removed. The observing bandwidth is relatively narrow, so this will not be a good determination unless the intrinsic

RM of the object is large, especially at high frequencies. In almost all cases, the systematic variation in PPA across the band was less than 15°, and for these cases, the depolarization is at most a few percent. In fact, if $RM \neq 0$ introduces a total change across our 28-MHz band of $\Delta\chi = 30°$, the resulting depolarization is only 5%, not the 25% suggested by equation 2.20. This corresponds to an RM of 300 at 1410 MHz, 60 at 820 MHz, and 20 at 575 MHz. Frequently, random variations and systematic trends which did not follow λ^2 were comparable or larger than any linear trend. For PSR B1821−24, the RM at 820 MHz was found to be somewhere between 60 and 100. This causes only slight depolarization at this frequency, due to the narrow bandwidth, but has a significant effect at 575 MHz, where we had been previously unable to measure the RM. A rotation measure of 80 was applied to the 575-MHz data. This resulted in less depolarization of the profile, and any remaining trend of PPA across the band was less than 10°.

The angle offsets determined above were applied to each scan prior to temporal alignment and adding of the profiles. In some cases, the PPA offset between data sets was insufficiently determined, due to low S/N or small linear polarization, and no offset was applied before averaging.

In order to properly align the data temporally, TOAs (pulse arrival times) were generated for each scan by cross-correlation with a template. At each frequency, these were then compared with the pulsar timing model used to take the observations, using the TEMPO timing package developed at Princeton (Taylor & Weisberg 1989). If the timing residuals were small, then the data were averaged with no further alignment. If significant timing residuals remained, then TEMPO was used to fit for a new timing model for those observations. This new model was then used to align and average the polarization data. In some cases, insufficient information was available to obtain a new timing model. In these cases, sub-averages of several scans were created where no drift in pulse phase was expected. These were then aligned and averaged by cross-correlation. In some cases, a small portion of the data was very much stronger, due to interstellar scintillation. In these cases, only the data with the highest S/N were included. In a few cases, the resolution of the data was not the same for all observations. These data were interpolated to the same number of bins prior to their addition.